We are IntechOpen,
the world's leading publisher of Open Access books
Built by scientists, for scientists

6,900
Open access books available

185,000
International authors and editors

200M
Downloads

154
Countries delivered to

Our authors are among the

TOP 1%
most cited scientists

12.2%
Contributors from top 500 universities

CLARIVATE ANALYTICS
BOOK CITATION INDEX
INDEXED

WEB OF SCIENCE™

Selection of our books indexed in the Book Citation Index
in Web of Science™ Core Collection (BKCI)

Interested in publishing with us?
Contact book.department@intechopen.com

Numbers displayed above are based on latest data collected.
For more information visit www.intechopen.com

Recent Advances in Silicon Photodetectors Based on the Internal Photoemission Effect

Maurizio Casalino

Additional information is available at the end of the chapter

Abstract

Silicon technologies provide an excellent platform in order to realize microsystems where photonic and microelectronic functionalities are monolithically integrated on the same substrate. In recent years, a lot of passive and active silicon photonic devices have been optimized to work at telecom wavelengths where, unfortunately, silicon has a neglectable optical absorption due to its bandgap of 1.12 eV. Although silicon cannot detect wavelengths above 1.1 μm, in recent years, tremendous advances have been made in order to make it suitable for operation in the near-infrared spectrum. One of the approaches is to take advantage of the internal photoemission effect through a Schottky junction where a metal absorbs the incoming radiation and emits hot carriers into silicon making sub-bandgap detection possible. The present chapter describes the more recent advances in the field of the silicon photodetectors based on the internal photoemission effect showing as devices based on new emerging materials and complex nanostructure are leading this family of device to compare favorably with the well-established technologies commonly used for telecom wavelengths based on germanium and III–V semiconductors.

Keywords: silicon, internal photoemission effect, photodetectors, near-infrared, graphene

1. Introduction

Silicon (Si) photonics is a discipline of paramount importance in the field of integrated optics, and, nowadays, new Si-based commercial products are already available on the

market [1, 2]. Although Si photodiodes are commonly realized to operate at visible wavelengths, their development at wavelengths of interest for telecommunications is not a trivial task to reach because Si is transparent at wavelengths above 1.1 μm. Conventional near-infrared Si-based PDs are based on the integration with III–V compound semiconductors as: InGaAs [3, 4], Ge [5], and SiGe [6]. Concerning InGaAs, a hybrid approach [7] is commonly followed because of the high lattice mismatch between InGaAs and Si (8.1%) making the monolithic integration with Si very difficult [8]. On the other hand, the growth of Ge on a Si substrate can be traditionally obtained with a two-step epitaxial growth technique [8, 9] in order to realize a buffer layer where a pure crystalline Ge can be epitaxially grown on Si substrates [10]. However, the requirement for a buffer layer that causes problems in both thermal budget and planarity [11, 12] prevents its monolithic integration on Si. Indeed, even if Si four-channel optical receivers based on GePDs have been successfully realized by both Intel [13] and Luxtera [14], it is worth noting that they are only flip-chip mounted to a Si electronic circuitry. In alternative, there has been progress in fabricating SiGe-based PDs. SiGe has been considered as semiconductor because it is still implemented in the CMOS process flow [6], but, unfortunately, the Ge content of the available layer is estimated to be 25–35% [15], and consequently, the detection wavelength is lower than 1200 nm [16]. In order to circumvent all these drawbacks, many approaches have been followed to realize silicon compatible PDs [17]. In particular, very promising is the approach based on the internal photoemission effect (IPE), that is, the exploitation of photon-assisted transmission of hot carriers across a potential barrier at metal-semiconductor interfaces. In the last decade, much effort has been focused on this field, and both impressive results and new structures have been reported. Indeed, IPE has been combined with nanoscale metallic structures, including metal stripes supporting surface plasmon polaritons (SPPs) [18, 19], Si nanoparticles (NPs) [20], metallic gratings [21], and antennas [22]. In addition, IPE has been combined with new structures based on two-dimensional materials (like graphene) able to replace metal in the Schottky junction [23]. After these research processes, IPE-based Si PDs show the potentialities to compare favorably with Ge-based devices, while also offering new advantageous characteristics. Indeed, IPE-based PDs are very fast thanks to the unipolar nature of the Schottky junction, and they have already shown the capability to be monolithically integrated with Si-based charge coupled devices for infrared applications [24]. IPE-based Si PDs were already summarized in a previous work of some years ago [25].

In the present chapter, the huge advances made in this field, are reported. In the first section, IPE theory will be elucidated in detail taking advantage of the new recent developments. Then, the main structures reported in the literature, and the most significant results obtained in recent years will be reviewed and discussed, comparing the performance of devices based on the different approaches. In particular, the second section will illustrate the state-of-the-art of the main both surface-illuminated and waveguide IPE-based Si PDs reported in literature, while the third section will be dedicated on devices able to combine IPE with plasmonic effects. Finally, in the fourth section, the potential of new devices taking advantage of both newly emerging materials and smart structures will be addressed.

2. Internal photoemission theory

IPE is the optical excitation of electrons in the metal to energy levels above the Schottky barrier and then the transport of these electrons to the energy bands of the semiconductor. A band diagram for a metal/p-Si junction is sketched **Figure 1**.

It is well-known that IPE is typically a very weak effect due to many factors: (1) the low absorption due to high reflectivity of the metal layer, (2) the conservation of momentum during carrier emission over the potential barrier which lowers the carriers emission probability into semiconductor, (3) the excitation of carriers lying in states far below the Fermi energy, which get very low probability to overcome the Schottky barrier. The result is that IPE-based devices are characterized by low responsivity R (i.e., the ratio between the photogenerated current I_{ph} and the incoming optical power P_{inc}):

$$R = \frac{I_{ph}}{P_{inc}} = \frac{\lambda\,[\,nm\,]}{1242} \cdot \eta_e \tag{1}$$

where λ is the wavelength of the incident photon expressed in nm, and η_e is the external quantum efficiency of the device, that is, the number of charge carriers collected per incident photon. Alternatively, the number of carriers collected per absorbed photons is called the internal quantum efficiency η_i.
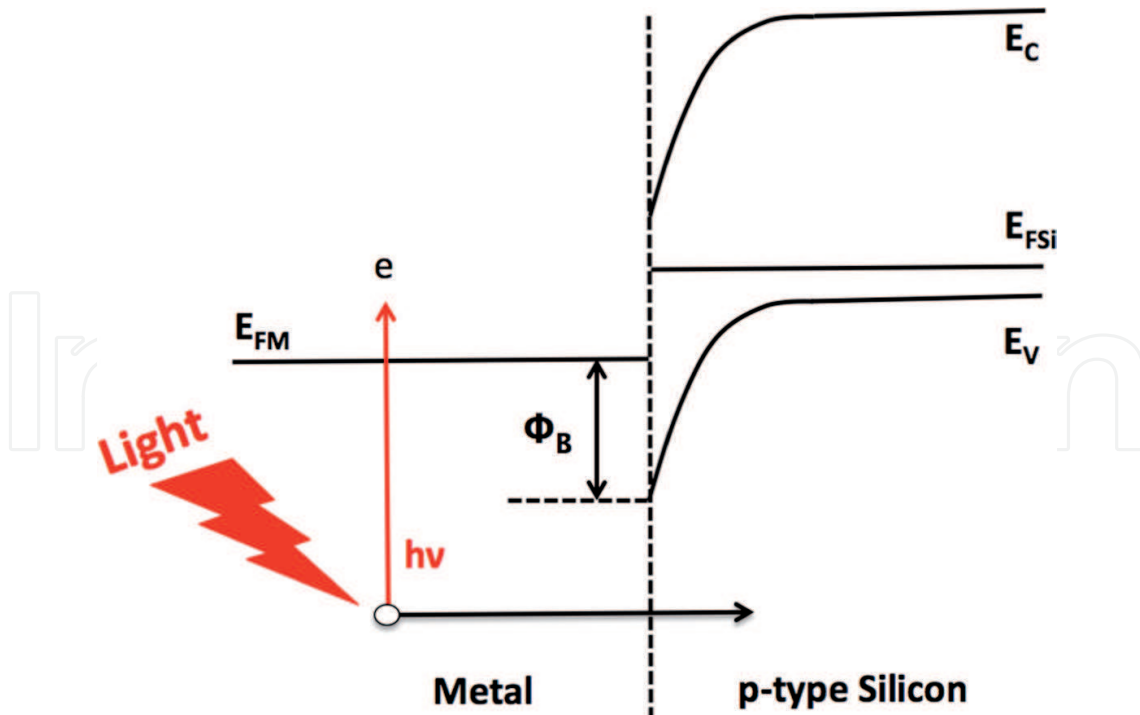
Figure 1. Energy band diagram for a metal/p-type Si junction (E_{FM} and E_{FSi} are the metal and Si Fermi level. E_C and E_V are the conduction and valence band energy of Si and ϕ_B is the Schottky barrier of the metal/p-Si junction.

Fowler described the first electron model concerning electron photoemission from metal into vacuum in the 1931 [26]. Subsequently, in the 1960s, Cohen et al. [27] modified the Fowler's model in order to take into account the carrier photoemission from a metal into a semiconductor, elaborating the commonly used formula:

$$\eta_i = C \cdot \frac{(h\nu - \phi_B)^2}{h\nu} \tag{2}$$

where ϕ_B is the Schottky barrier, $h\nu$ is the energy photon, $C = 1/8(E_F + \phi_B)$ is named the quantum efficiency coefficient, and E_F is the metal Fermi level. In this context, it is worth noting that Eq. (2) was obtained under the zero temperature approximation and for thick metal films.

Subsequently Elabd and Kosonocky reviewed the IPE model in order to obtain better agreement with the experimental data [28] and, always under the zero temperature approximation, they obtained approximately the same Eq. (2) but characterized by a different quantum efficiency coefficient that results $C = 1/8\phi_B$. In addition, the authors extended the photoemission model to the case of thin metal films by introducing a multiplicative gain factor arising from the increased escape probability of the hot carriers into the metal due to the scattering with metal surfaces [28]. In the last years, many other authors have investigated IPE theory and new physical models more and more complex have been proposed [29–31]. Recently, Scales and Berini extended the Elabd and Kosonocky's theory in order to take into account of the escape probability through a double Schottky barrier [32]. A very intriguing approach was proposed by Vickers, who derived a theoretical model in which the estimation of the internal quantum efficiency η_i is given by the product of two factors [33]:

$$\eta_i = F(\phi_B) \cdot P(d) \tag{3}$$

where the Fowler factor F is the fraction of the excited carriers having appropriate momentum and energy to overcome the potential barrier, P is a scattering term taking into account the probability that one of these excited (hot) carriers will be emitted over the potential barrier after scattering by cold carriers and the metal boundary surfaces, d is the metal thickness, and ϕ_B is the junction potential barrier. The main advantage of the Vickers model is that the zero temperature approximation is removed making it valid at any temperature. Indeed, the factor F incorporating the temperature dependence is shown in the following formula:

$$F = \frac{1}{4 E_F h\nu} \left(\frac{(h\nu - \phi_B)^2}{2} + (k_B T)^2 \left\{ \frac{\pi^2}{6} + \sum_{i=1}^{\infty} \frac{1}{i^2} \left(-e^{\frac{h\nu - \phi_B}{k_B T}} \right)^i \right\} \right) \tag{4}$$

where k_B ant T are the Boltzmann constant and the absolute temperature, respectively. It is worth noting that, in the limit $T \rightarrow 0$, Eq. (4) reduces to the well-known Eq. (2). Recently, Casalino [34] showed that by making a change of variables $m = (h\nu - \phi_B)/k_B T$ and putting in evidence the factor $(k_B T)^2$ in (4), it is possible to define a F^* factor as:

$$F^* = \frac{4 E_F h\nu}{(k_B T)^2} F = \left(\frac{m^2}{2} + \frac{\pi^2}{6} + \sum_{i=1}^{\infty} \frac{1}{i^2} \left(-e^{-m} \right)^i \right) \tag{5}$$

Three terms of Eq. (5): $m^2/2$, $\pi^2/6$ and the polylogarithm function $\sum_{i=1}^{\infty} \frac{1}{i^2} (-e^{-m})^i$ have been plotted in **Figure 2** by varying m between 10^{-6} and 2×10^5 in order to understand the weight that any term plays into (5). It is possible to estimate that F^* approaches $m^2/2$ within 10% for $m \geq 5.43$, within 5% for $m \geq 7.91$ and within 1% for $m \geq 18$.
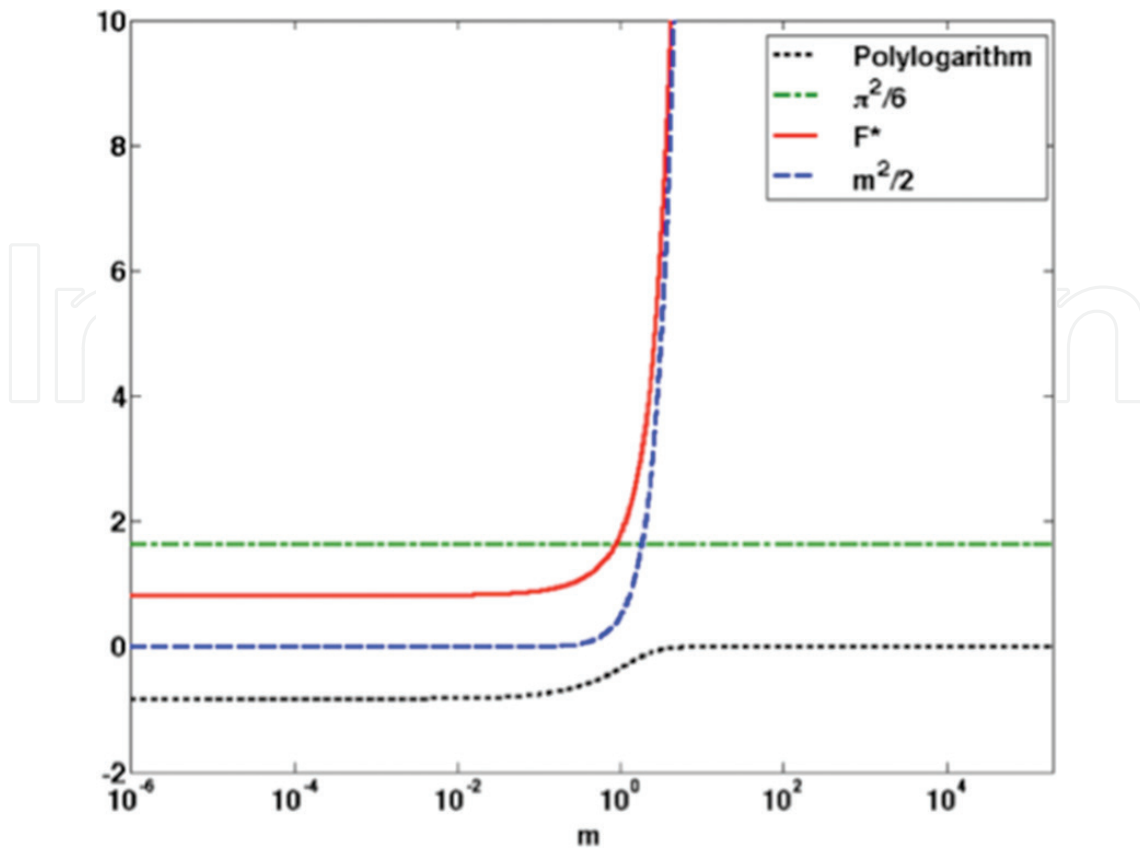
Figure 2. Plot of the F^* factor as a function of m. Three terms forming F^*: $m^2/2$, $\pi^2/6$ and the polylogarithm function are reported, too. X-axis is plotted on log scale.

Most important, Casalino found that F^* approaches $m^2/2 + \pi^2/6$, that is, it is possible to neglect the polylogarithm term and to reduce Eq. (4) to the following Eq. (6) [34]:

$$F = \frac{1}{8\,E_F\,h\nu}\left((h\nu - \phi_B)^2 + \frac{(k_B\,T\pi)^2}{3}\right) \qquad (6)$$

within 10% when $h\nu - \phi_B \geq 0.035$ eV, within 5% when $h\nu - \phi_B \geq 0.046$ eV, and within 1% when $h\nu - \phi_B \geq 0.074$ eV. It is worth noting that Eq. (6) is a slight modification of Eq. (2) but can be used also at room temperature in the limit of the aforementioned errors.

On the other hand with reference to Eq. (3), the scattering term P allows extending IPE theory to a thin film where the escape probability of carriers excited in the metal is increased. Because the P term derived by Vickers is further complex, he proposed the following analytical approximation, very simple but with no physical meaning [33]:

$$P = \frac{L^*}{d} \cdot \sqrt{1 - e^{-\frac{d}{L^*}}} \qquad (7)$$

where L^* is the mean free path in the metal, and d is the metal thickness. Eq. (7) is valid for thin films but in the limit $d/L^* > 0.2$. By following the same line of reasoning, more recently Casalino introduced the following Eq. (8) able to extend the operating range in the limit $d/L^* > 0.002$ [34]:

$$P = \frac{L^*}{d} \cdot \left(\sqrt{1 - e^{-\frac{d}{L^*}}} + 0.1 \cdot e^{-4.1\frac{d}{L^*}} \right) \tag{8}$$

Because the lower the metal thickness the higher the scattering term P, there is always an advantage to work with very thin metal thickness to the point that it was recently to proposed to replace metal with two-dimensional material such as graphene able to form Schottky junction with Si [23]. Finally, it should be mentioned that device efficiency can also be increased by applying a reverse bias to the Schottky junction, and this increase is due to the lowering of the Schottky barrier ϕ_B when a reverse bias is applied to the junction (image-force effect [35]).

It is worth noting that in this section we have focused only on the device efficiency of the PDs because it is the Achilles' heel of all IPE-based devices. However, many others figures of merit are useful in order to compare different PDs: bandwidth, noise equivalent power (NEP), and voltage operation are the main specifications of any commercial PD datasheet, and their definitions can be found everywhere [36].

3. Surface-illuminated and waveguide Schottky PDs

Schottky surface-illuminated PDs are typically less responsive than Schottky waveguide PDs where the optical power is confined close to the metal-semiconductor interface and can be absorbed along its propagation. However, in some cases, the surface-illuminated structures are the only option: for instance, in imaging applications where the vision can be improved in critical conditions (such as smoke and fog) thanks to reduced scattering at NIR wavelengths [37] or in reflectography applications where the transparency of most pigments to NIR wavelengths has been used to investigate ancient paintings [38]. Historically, surface-illuminated Schottky PDs have been used in the field of Schottky-barrier infrared focal-plane array (FPA) technology [24]. PtSi/pSi PD is the most popular surface-illuminated Schottky-barrier device, commonly used for detection in the 3–5 μm spectral range [39]. However, this device is characterized by two main drawbacks: low quantum efficiency (about 1%) and low operating temperature requirements (77 K or below). In order to overcome these drawbacks, in 2006, Casalino et al. proposed to incorporate a Schottky junction inside a Fabry-Perot optical microcavity in order to enhance the device efficiency at both near-infrared wavelengths and room temperature [40, 41]. Subsequently, in 2012, after a first experimental proof-of-concept demonstration [42, 43], the same authors fabricated and characterized a new surface-illuminated Schottky device based on a resonant cavity Fabry-Perot structure. The device was formed by a dielectric bottom mirror, a metallic top mirror and, in the middle, a silicon cavity [44]. The dielectric bottom mirror was a distributed Bragg reflector (DBR) formed by alternating $\lambda/4$-layers of amorphous hydrogenated silicon (a–Si:H) and silicon nitride (Si_3N_4), while the top mirror was realized by means of a copper (Cu) layer able to work as both an absorber and an optical mirror at the same time. It was demonstrated that, when the DBR mirror reflectivity approaches the reflectivity of the metallic top mirror, that is, when critical coupling conditions are fulfilled, the maximum responsivity can be obtained at the cavity resonance wavelengths. The critically coupled Cu/pSi Fabry-Perot PD exhibited a maximum responsivity of 0.063 mA/W around

1550 nm and measurements of junction capacitance in the pF range encouraged the pursuit of greater bandwidth making possible to operate at several GHz. On the other hand, the dark current density is reported to be as high as 28 mA/cm^2 at −1 V. More recently, Desiatov et al [45]. have demonstrated surface-illuminated Aluminum(Al)/Si Schottky PDs at near-IR wavelengths based on pyramidally shaped devices created in Si by potassium hydroxide (KOH) anisotropic etching. The advantage of KOH etching is that it is possible to fabricate plasmonic devices with a nanometric active area, without requiring sophisticated equipments such as electron beam lithography (EBL) or focused ion-beam (FIB). SEM micrographs of the fabricated device are shown in **Figure 3(a)** and **(b)**. The Si pyramids arranged in an array structure work as efficient and broadband light concentrators able to collect the light from a large area and to confine it into a small active pixel area, thereby providing high responsivity and low dark current at the same time. The responsivity of the device at −0.1 V was found to be 5, 12, and 30 mA/W for incident optical wavelengths of 1550 nm, 1300 nm, and 1064 nm, respectively. Moreover, the device showed a dark current of 80 nA at −0.1 V. The authors claim in this work that the efficiency is enhanced, not only by the increased absorption, but also by the nanoscale apex of the pyramid able to increase the escape probability from Al into Si.

Concerning waveguide Schottky PDs, in 2008, Zhu et al. [46] described the first nickel silicide (NiSi) Schottky PD integrated into a silicon-on-insulator (SOI) waveguide working at both NIR wavelengths and at room temperature. In this case, the author reports a responsivity, bandwidth, and dark current of 4.6 mA/W, 2 GHz and 3 nA at −1 V of reverse bias applied,
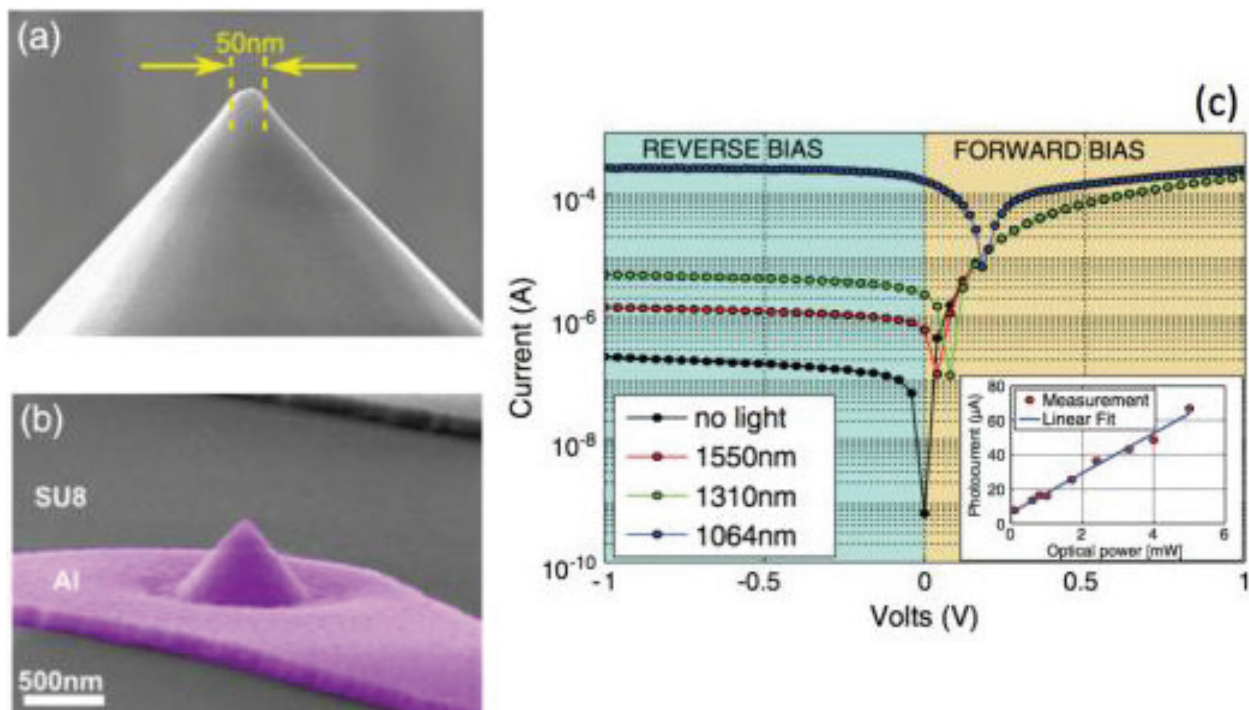
Figure 3. SEM micrograph of the device reported in [45]: (a) formation of the nanoapex in the Si pyramid and (b) final fabricated device. (c) I–V measurements of the pyramid Schottky device at constant optical power for three different wavelengths. The inset shows the photocurrent versus optical power for 1550 nm wavelength.

respectively. A similar device from the same research group, but based on a metal-semicon-ductor-metal (MSM) configuration, shows both higher responsivity and larger dark current [47]. It is worth noting that in the aforementioned guiding structures, the absorbing metal is always deposited along the direction of the propagating light, but another possibility is that the active metal layer is placed on the vertical exit surface of the output waveguide, that is, normal to the propagating beam.

This proposed PD design is reported in [48], and it is based on an asymmetric MSM junction integrated onto a SOI substrate. The active metal is copper (Cu) that results in contact with Si only on the vertical exit wall of the optical waveguide. In practice, Cu works as a mirror (as well as an active absorbing layer), enabling the possibility of fabricating an integrated cavity if a second mirror is realized on the waveguide (for instance by means of deep trenches) in order to get a substantial shrinkage of the footprint together with an increase in the device perfor-mance. The integrated PD was characterized by a responsivity value at 1550 nm of 0.08 mA/W and a dark current of 10 nA at −1 V. In 2013, Casalino et al. proposed an optimized version of this device showing the possibility of tackling the typical responsivity/dark current trade-off [49, 50]. Indeed, in [50], it was shown that, by taking advantage of a small contact area of about 3 μm^2, it was possible to increase the reverse bias applied even up to 21 V while maintaining a limited dark current value of only 2.2 nA. The increase in reverse voltage allows reducing the Schottky barrier height (due to the image force effect [35] mentioned in Section 2), increas-ing the responsivity up to 4.5 mA/W. In addition, an experimental bandwidth of 1 GHz was demonstrated. Finally, the Schottky PD proposed shows the potentialities to work at longer wavelengths than NIR (i.e., wavelengths in the range 2–3 μm) [50].
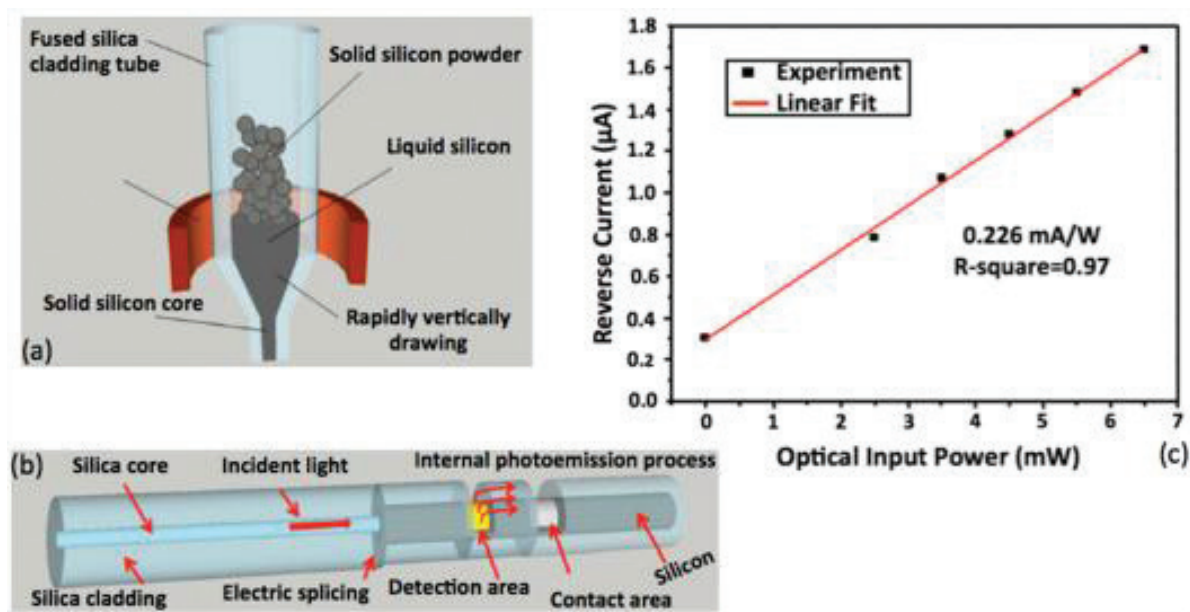
Figure 4. (a) A schematic illustration showing the fabrication process for making the Si-cored fiber and (b) the Schottky PD directly integrated on the Si-cored fiber described in [53]. (c) Measured photocurrent versus optical power from a 1550 nm laser.

In this section, we believe that other two structures proposed in the current literature deserve to be mentioned. The first concerns the possibility to combine Schottky PDs with microring resonators, and these structures have been investigated theoretically in the current literature [51, 52] providing encouraging results; however, no experimental validation has been carried out to so far. The second is reported in [53] where a very intriguing in-line IPE-based Si PD was fabricated directly on an optical fiber. In particular, an Au Schottky layer was placed directly on the Si core of a non-conventional optical fiber fabricated by starting from polycrystalline n-type Si powder, firstly packed in a fused silica tube, and then melted at an appropriate temperature as shown in **Figure 4(a)** and **(b)** [53]. The authors report a responsivity and dark current combination of 0.226 mA/W and 0.3 μA, respectively, at −0.45 V for a wavelength of 1550 nm as shown in **Figure 4(c)**. This device could become very interesting in the field of Lab-on-Fiber technology.

4. Surface-plasmon Schottky PDs

Surface-plasmon Schottky PDs allow combining IPE with the excitation of surface plasmon polaritons (SPPs) in a waveguide provided of a proper metal layer [54]. In other words, when the SPP is excited, it will be absorbed during its propagation along the metal stripe deposited on the Si waveguide. Absorbed photons will generate photoexcited carriers able to be emitted through the Schottky junction into Si making the sub-bandgap detection possible also at NIR wavelengths in agreement with the internal photoemission mechanism. The P. Berini's group has theoretically [55] and experimentally [18] investigated the performance of Schottky PDs integrated with Si-based waveguides supporting SPPs.

A first proposed structure is based on an Au stripe deposited on p-Si to form a Schottky contact [18, 19]. The authors demonstrate that the plasmonic mode excitation, localized at the Au/p-Si interface, occurs at NIR wavelengths under both end-facet and top illumination. In particular, under end-facet illumination, the measured responsivities in an asymmetric 1.5-μm-wide, 40-μm-long, and 40-nm-thick Au stripe waveguide were 0.942 and 0.941 mA/W at 1310 nm and 1550 nm, respectively, and at −0.1 V of reverse bias applied. On the contrary, under top illumination, the measured responsivity in an asymmetric 6.5-μm-wide, 40-μm-long, and 40-nm-thick Au stripe waveguide was 0.559 mA/W at the wavelength of both 1550 nm and −0.1 V of reverse bias applied. Moreover, the device dark current was in the μA range. Previously, the same authors reported on a similar device working under a strong reverse bias of −210 V close to the breakdown condition. The 2.5-μm-wide, 75-μm-long, and 135-nm-thick Au stripe on n-Si shows a responsivity of 2.35 mA/W at 1550 nm [56].

It is worth mentioning that the aforementioned devices are all based on asymmetric cladding configurations, and on the other hand, a symmetric cladding configuration, where the Au stripe is buried in Si [57, 58], gives the advantage of increased efficiency thanks to the emission through two Schottky junctions [32]. Even if no experimental validation has been performed in symmetric cladding SPP Si PDs so far, Knight et al. [59] proved increased responsivity for plasmonic nanostructures embedded in Si. Indeed, Ti (2 nm)/Au (35 nm) planar nanowires
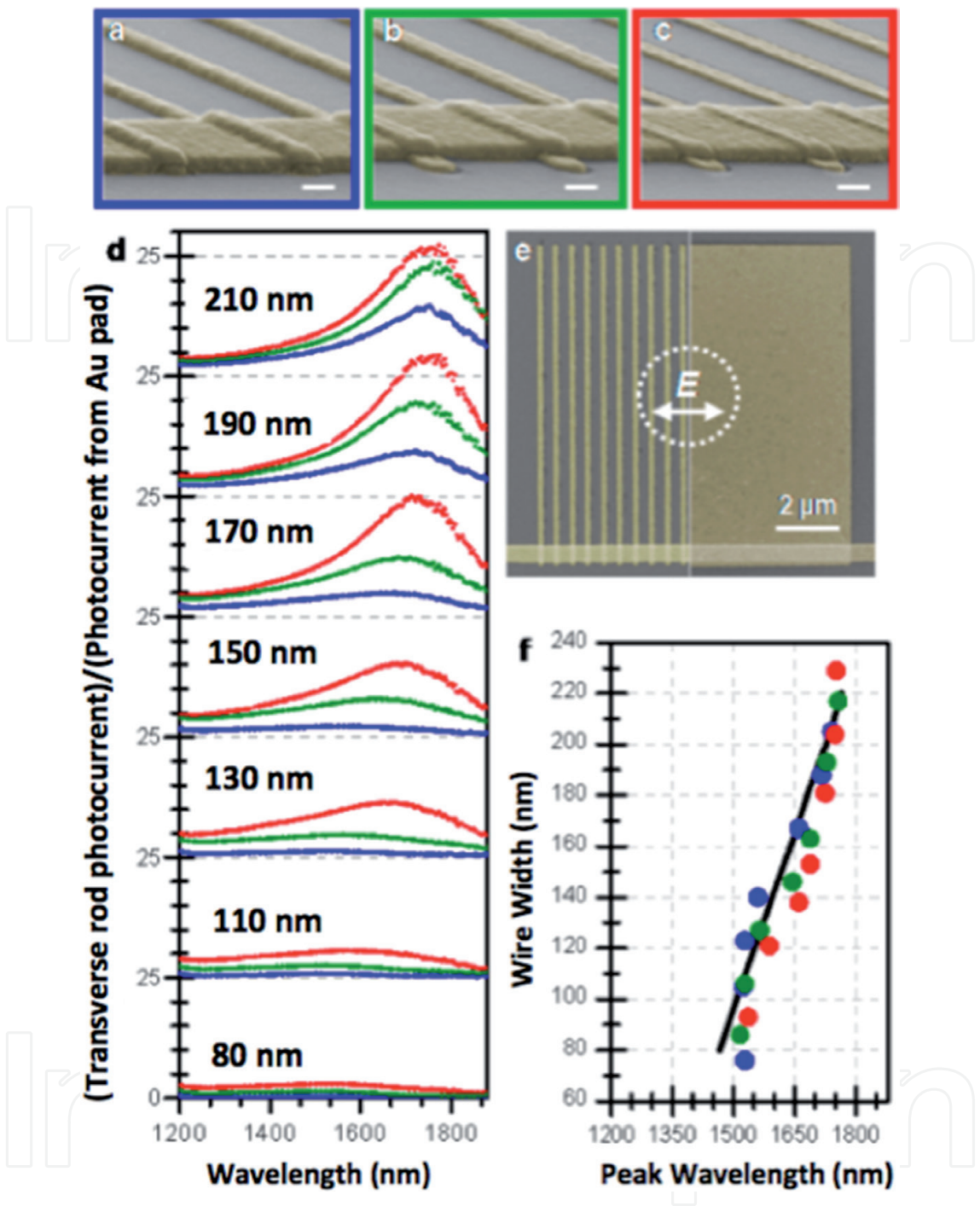
Figure 5. (a–c) Three representative SEM images of devices with widths of 120 ± 10 nm embedded about: 5 nm (blue), 15 nm (green), and 25 nm (red) into the silicon substrate. Scale bars are 100 nm. (d) Measured photocurrent spectra for increasing widths, where each spectrum is the photocurrent from (e) a nanowire array normalized to the response from a solid Au pad. The dotted white circle indicates the laser spot FWHM of 3 μm. Scale bar is 2 μm. (f) Calculated absorption peak wavelengths (black line) agree closely with experimentally observed enhancement peaks.

arranged into a 10 μm × 10 μm array were embedded in Si to a depth of 5 nm, 15 nm, and 25 nm in such a way that not only the flat surfaces but also the lateral surfaces of the planar nanowires are able to emit photoexcited carriers through the Schottky junctions (**Figure 5**).

The authors prove that an increased photocurrent can be achieved with respect to nonembedded plasmonic elements, in other words the higher the embedding depth, the higher the responsivity, and this trend was most clearly observable for the nanowires with the widest transverse dimensions. Indeed, devices based on the highest width to thickness ratio exhibited a photocurrent of about 25 times greater than the non-embedded structures. For incident light polarized transverse to the length of the nanowire, the maximum reported responsivity was 65 μA/W at 1550 nm. The authors attribute the responsivity enhancements to the increased carrier probability emission occurring through the three metal/Si interfaces. The embedded Schottky junctions and the main results reported in [59] are reported in **Figure 5**. In the 2012, Goykhman et al. demonstrated a NIR Al/Si Schottky PD integrated with a submicrometer Si waveguide fabricated taking advantage of the standard microelectronic LOCOS (Local Oxidation of Silicon) technique [60]. The 320 nm × 1000 nm Al active area in contact with the Si forms a Schottky PD with responsivity of about 12.5 mA/W at 1550 nm and −0.1 V bias, while the leakage current is only 30nA. The measured responsivity is about two orders of magnitude higher than that published two years earlier by the same authors for a similar device [61], and they attribute the enhanced responsivity to the presence of plasmonic effects due to the surface roughness at the boundary between the Al and the Si. In the same year, Zhu et al. demonstrated PDs based on nickel silicide nanoparticles embedded in the space charge region of a waveguide p-n Si junction [20]. While the idea of enhancing the IPE by using nanoparticles (NPs) was already explored in the past [62, 63], it is worth noting that the previously reported structures were able to operate only at cryogenic temperatures (77 K) and at wavelengths shorter than those required for telecommunications [64, 65]. The enhanced responsivity of PDs based on NPs is ascribed both to the increased light absorption due to the excitation of localized surface plasmon resonance (LPSR) and to the increased emission probability of the excited carriers due to the spherical shape of the NPs [66]. On the other hand, the device proposed in [20] is able to work at both room temperature and 1550 nm and its fabrication is very interesting: the junction was realized by depositing a ~1-nm-thick titanium (Ti) film and a ~3-nm-thick nickel (Ni) film on p-Si, and a subsequent rapid thermal annealing process at 200°C for 30 s produces the nickel silicide (NiSi). After removing the un-reacted metal using a proper etching solution (Piranha at 90°C), a 200-nm-thick film of amorphous Si was deposited, followed by phosphorus implantation and a rapid thermal annealing at 700°C for 5 min in order to get the dopant activation. It is worth noting that during this rapid thermal process, the Ni-silicide agglomerated to form NPs. At the same time, the amorphous Si crystallizes to form polycrystalline Si. The measured responsivity at room temperature depends on both wavelength and polarization, and the maximum value is 30 mA/W for −5 V and TE polarization. Finally, a dark current density and bandwidth of 2.84 A/cm² and 6 GHz at −5 V were reported, respectively. In [67] are reported Schottky PDs based on Au nanorods randomly distributed on a 30-nm-thick Au film deposited on Si. Various nanorods lengths ranging from 50 to 100 nm were considered, while their diameter was 10 nm. The authors claimed that the Au nanorods are capable of inducing SPR excitation under illumination at 1300 nm and 1550 nm and an enhanced photocurrent with respect to the same devices without nanorods was demonstrated at zero bias. In 2011, Knight et al. [22] reported on strong optical absorption in a small active metal region due to the excitation of resonant plasmons in metallic nanoantenna. The PD consisted

of three hundred nanoantennas arranged in a 15 × 20 array. Each nanoantenna used 30-nm-high and 50-nm-wide rectangular Au nanorods with lengths ranged from 110 to 158 nm. Unfortunately, the PD responsivity depends on the complex optimization of several factors (the properties of the materials involved, the geometry, and the efficiency of the uppermost indium-tin-oxide electrical contact layer) and a very low responsivity of 10 μA/W and 3 μA/W at 1250 nm and 1550 nm were reported without reverse bias applied, respectively.

Another approach in order to obtain hot electron generation induced by plasmon modes was proposed by A. Sobhani et al. [21] who investigated the phenomenon of extraordinary optical transmission (EOT) in metallic gratings. The same plasmon modes that give rise to EOT also give rise to the excitation of electrons that can be emitted above the Schottky barrier into a semiconductor substrate as shown in **Figure 6**.

Gratings based on Au with different geometries were fabricated on n-type Si by using an interfacial layer of titanium in order to promote adhesion with Au. A measured maximum responsivity of 0.6 mA/W and 0.47 mA/W at 1300 nm and 1500 nm, for zero bias voltage, was demonstrated, respectively. Device measurements showed a drastic increase in responsivity
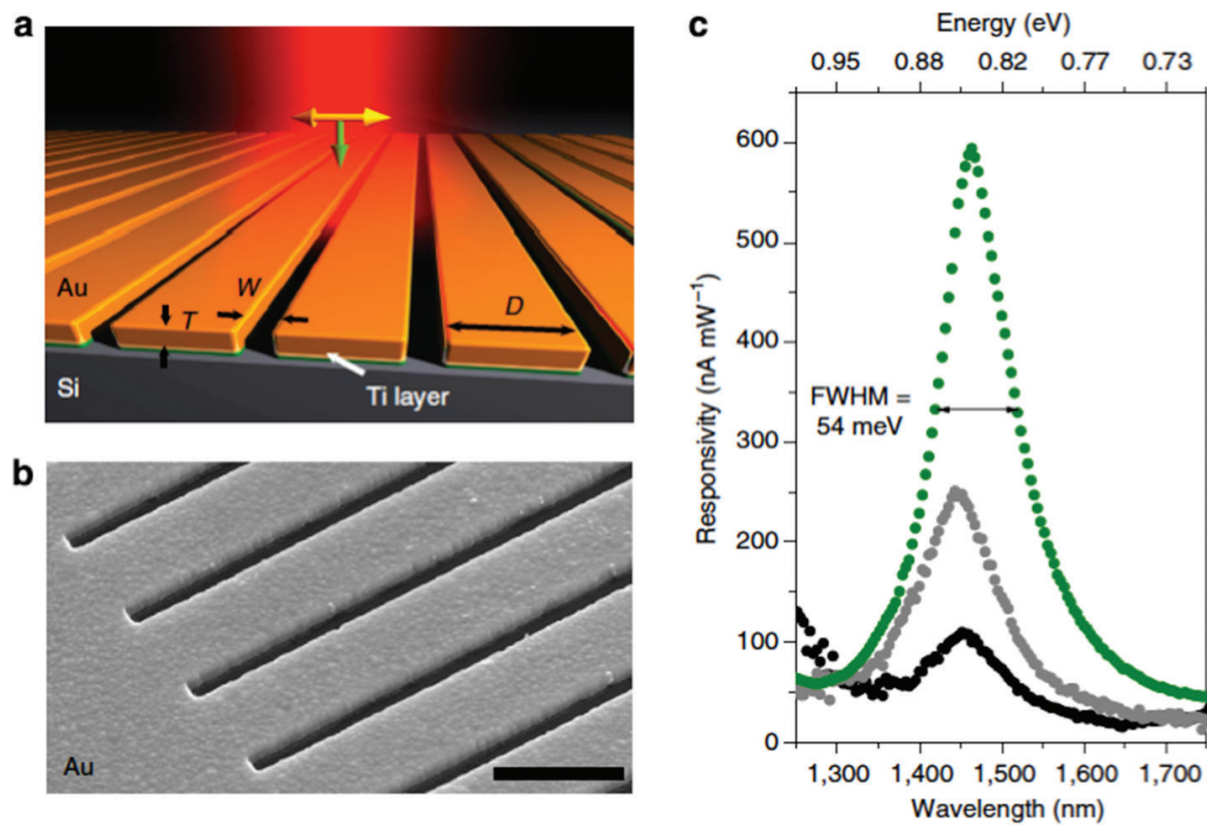
Figure 6. (a) Schematic of a gold grating on an n-type silicon substrate with a 2-nm Ti adhesion layer, oriented transverse to the laser polarization. Polarization of the incident laser and its k vector are represented with horizontal (yellow) and vertical (green) arrows, respectively. (b) Scanning electron microscopy image of gold grating structure with grating thickness (*T*)=200 nm, interslit distance (*D*)=950nm and slit width (*W*)=250 nm. For all structures the array measured 12 x 12 mm. The scale bar is 1 mm. (c) Photocurrent responsivities of grating-based photodetectors for three different gold layer thicknesses, T=93 nm (lower black curve), 170nm (grey curve in the middle) and 200nm (higher green curve), showing a strong intensity dependence on grating thickness.

with respect to structures based on nanoantennas previously mentioned. This increase mainly arises from the possibility to design the grating geometry in such a way to generate hot electrons primarily near the Schottky interface. Finally, this approach allows tuning the responsivity peak over a broad wavelength regime ranging from 1295 to 1635 nm, simply by changing the grating geometry.

Concerning the possibility to detect in a wide range of NIR wavelengths, in 2014 Nazirzadeh et al. [68] demonstrated Si Schottky PDs, operating in the 1200–1600 nm spectrum, based on Au nanoislands able to plasmonically enhance the sub-bandgap photon generation and collection. In this work, randomly distributed Au nanoislands on Si surface were realized by annealing a continuous thin Au layer at temperatures of 300°C, 450°C, and 600°C, respectively. The structure annealed at 450°C showed the highest responsivity of 2 mA/W at 1300 nm, while a dark current of about 30 μA at −1 V was reported. On the contrary, a device annealed at 300°C showed a responsivity of 0.6 mA/W at 1550 nm, while a dark current of about 100 μA at −1 V was demonstrated. The main advantage of the proposed PD is that all nanostructures were realized without requiring high-resolution electron beam lithography (EBL). Very recently, in 2016, Muehlbrandt et al. reported a novel plasmonic internal photoemission detector (that authors name with the PIPED acronym) characterized by a Si waveguide where the two sidewalls are metallized by two different metals: gold (Au) and titanium (Ti) [69]. The Au-Si-Ti waveguide is able to guide SPPs dissipating their energy mainly at Ti/Si interface because Ti is characterized by a larger imaginary part of the complex refractive index with respect to Au. In this work, authors demonstrate that when an external positive DC-bias voltage is applied (positive polarity from gold to titanium), the band diagram of the Au-Si-Ti structure changes in such a way that IPE at 1550 nm can occur over the Ti/Si Schottky barrier. The structure based on asymmetric Au-Si-Ti waveguides with a width of 75 nm and a length of 5 μm shows a responsivity at 1550 nm and dark current of 0.126 A/W and ~10 μA, respectively, at a bias voltage of 3.25 V. Finally, the detector exhibits optoelectronic bandwidths of at least 40 GHz.
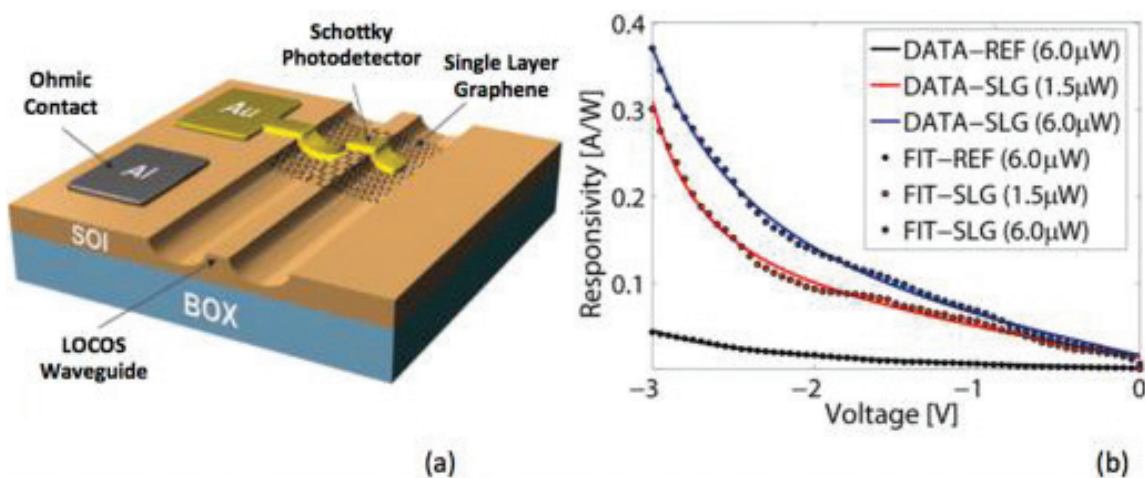
5. Graphene/Si Schottky PDs

Deep investigations have been realized on graphene since its discovery in 2004 [70]. This is because electrons in graphene behave as massless two-dimensional particles leading to a wide absorption over wavelengths from the ultraviolet to the infrared thanks to both inter-band and intra-band transitions [71, 72]. In the field of the photodetection, this property is of fundamental importance because the semiconductors used for realizing PDs are characterized by a limited absorption range. This is because graphene-based PDs are nowadays one of the most studied photonic devices over a broadband range of wavelengths, in particular at NIR. It is well-known that graphene forms a Schottky junction with Si [73], and it results a good candidate for the realization of IPE-based devices due to its very low thickness that promises to increase the emission probability of the photoexcited carriers over the Schottky junction. In 2013, Amirmazlaghani et al. reported on an exfoliated graphene/Si Schottky PD operating at 1550 nm [23] showing a maximum experimental responsivity of 9.9 mA/W at

both 1550 nm and −16 V. On the other hand, the measured dark current was 2.4 μA. A key point of the work is that the proposed device shows an experimental responsivity higher than that predicted by the traditional IPE theory. The authors explain the discrepancy by claiming that IPE theory should be totally revised when two-dimensional materials are considered, and they propose an alternative model in a good agreement with the experimental results. It has been shown that the insertion of a graphene monolayer in between the metal and the semiconductor provides an IPE enhancement [74] and very recently Levy et al. have proposed a phenomenological model able to explain physics behind this enhancement [75].

Recently Goykhman et al. demonstrated a NIR Schottky PD integrated with a SOI waveguide based on silicon-graphene junctions where graphene is grown by chemical vapor deposition CVD system [74]. Device is shown in **Figure 7**.

In particular, the rib waveguide was coupled to a single layer graphene (SLG)/Au contact able both to form a Schottky junction with Si and to support surface plasmonic modes that confined the optical beam to the SLG/Si interface. The PD length was ~5 μm, while the Si waveguide width was 310 nm. A responsivity of 0.085 A/W, at both, 1 V and 1550 nm, with respect to a dark current of 20 nA, was reported. Finally, the authors show that responsivity increases up to 0.37 A/W at a higher voltage of −3 V thanks to the combined effect of two processes: tunneling through the graphene/Si Schottky junction (thermionic-field emission, TFE [76]) and avalanche multiplication of within the Si depletion region.

Finally, Vabbina et al. have fabricated and characterized a very interesting two-dimensional Schottky PD working at 1440 nm [77]. The Schottky junction is realized by putting in contact the p-type molybdenum disulfide (MoS_2) with graphene, and the absorption mechanism is based on IPE: under illumination, photo-generated holes travel from the graphene into MoS_2 over the Schottky barrier. MoS_2 is a two-dimensional material attracting much interest due to its direct bandgap of 1.80 eV giving to the material semiconduc-

Figure 7. (a) Schematic metal-SLG-Si Schottky PD proposed in [74]. (b) Responsivity of metal-SLG-Si and reference metal-Si PDs for a reverse bias ranging from 0 to –3 V (reference metal-Si device is used to demonstrate the key role of graphene). Solid lines show a fit of the bias dependent responsivity based on combined TFE and avalanche multiplication processes.

tor characteristic. The thin film graphene/MoS$_2$ junction was deposited on an oxidized silicon substrate. Few layers of MoS$_2$ were deposited by a combined sputtering-CVD technique, while graphene was synthesized by a CVD process. The authors show a Schottky barrier of 0.139 eV, and the spectral responsivity when the energy photon is higher ($hv > E_{gMoS2}$) and lower ($hv < E_{gMoS2}$) than MoS$_2$ bandgap (E_{gMoS2}) was experimentally measured at −2 V of reverse bias applied. In particular, author shows that when $hv > E_{gMoS2}$ a maximum responsivity of 0.52 A/W is observed at 590 nm, on the other hand, beyond 670 nm where $hv < E_{gMoS2}$, the photo-current is due to IPE from the graphene to the MoS$_2$. In this last case, a maximum responsivity and noise equivalent power (NEP) of 1.26 A/W and 7.8 × 10^{-12} W/√Hz were respectively reported at 1440 nm and −2 V. Measured dark current is about 300 μA at −2 V.

6. Conclusions

In this work, an overview of recent advances in the field of the near-infrared silicon photodetectors based on the internal photoemission effect has been presented. Firstly, we have described the detection mechanisms of the devices especially in light of the models proposed in the recent literature. Thereafter, a quantitative comparison of the state-of-the-art IPE-based silicon PDs including Si nanoparticles, metal stripes supporting SPPs, antennas, metallic gratings, and two-dimensional materials has been given and summarized in **Table 1**.

Device	Device type	Size	Responsivity	Bandwidth	Dark current/dark current density
Casalino et al. [44]	Surface-illuminated Fabry-Perot microcavity	100-μm-thick silicon cavity	0.063 mA/W @1550 nm (−0.1 V)	GHz range estimated	3.5 mA (−1 V)
Desiatov et al. [45]	Surface-illuminated Si pyramids	Pyramid apex ~50 nm	5 mA/W @ 1550 nm 12 mA/W @ 1300 nm 30 mA/W @ 1064 nm (−0.1 V)	–	80 nA (−0.1 V)
Casalino et al [50]	Waveguide	Active area ~3 μm^2	4.5 mA/W @ 1550 nm (−21 V)	1 GHz	2.2 nA (−21 V)
Berini et al. [18]	Au strip supporting SPPs	Asymmetric 1.5-μm-wide 40-μm-long 40-nm-thick strip	0.942 mA/W @ 1310 nm 0.941 mA/W @ 1550 nm (−0.1 V)	–	0.3 μA (−0.45 V)
Goykhman et al. [60]	Nanoscale bus waveguide	Al active area 0.32 μm × 1 μm	12.5 mA W @ 1550 nm (−0.1 V)	–	30 nA (−0.1 V)

Device	Device type	Size	Responsivity	Bandwidth	Dark current/dark current density
Zhu et al. [20]	NPs supporting LPSR	Few nm NPs	30 mA/W @ 1550 nm (−5 V for TE polarization)	6 GHz	2.84 A/cm² (−5 V)
Knight et al. [22]	15 × 20 matrix of Au nanoantennas	30-nm-height 50-nm-width nanoantenna	10 μA/W @ 1250 nm 3 μA/W @ 1550 nm (No bias)	–	–
Sobhani et al. [21]	Au grating based on EOT	Different grating geometries (few hundreds of nanometers)	0.6 mA/W @ 1300 nm 0.47 mA/W @ 1500 (No bias)	–	–
Nazirzadeh et al. [68]	Au nanoisland	–	2 mA/W @ 1300 nm (450°C) 0.6 mA/W @ 1500 nm (300°C)	–	30 μA (450°C) 100 μA (−300°C) both −1 V
Muehlbr et al. [69]	Si waveguide with metallizedsidewalls (PIPED)	Asymmetric Au-Si-Ti 75-nm-wide 5-μm-long 300-nm-thick	0.126 A/W @ 1550 nm (3.25 V)	40 GHz (200 nm–wide 20 μm-long)	
Amirmaz et al. [23]	Surface-illuminated graphene/Si	–	9.9 mA/W @ 1550 nm (−16 V)	–	2.4 μA (−16 V)
Goykhman et al. [74]	Graphene integrated with a rib SOI waveguide	PD length ~5 μm Si waveguide width ~310nm	0.37 A/W @ 1550 nm (−3 V)	–	20 nA (−1 V)
Vabbina et al. [77]	Graphene/MoS$_2$ Schottky PD on oxidized Si	–	1.26 A/W @ ~1550 nm (−2 V)	–	300 μA (−2 V)

Table 1. Summary of selected IPE-based Si PDs at NIR wavelengths published since 2010.

The most part of IPE-based PDs have been realized for operation at telecom wavelengths, in particular at 1550 nm, and are characterized by a large GHz bandwidth thanks to the unipolar nature of the Schottky junction. In addition, a low dark current to the nA range has been obtained thanks to the use of plasmonic structures allowing strong absorption in a small metal layer in contact with silicon.

Historically, the main drawback of the IPE-based PDs is their external responsivity limited to the mA/W range at room temperature; this work put in evidence that taking advantage of both the integration of two-dimensional materials with silicon and plasmonic structures, a responsivity in the A/W range can be obtained. These values are comparable with the well-established near-infrared technologies based on germanium and III–V semiconductors and open the path to the investigation of more complex structures that can make the IPE-based Si Schottky PDs very promising to play a key role for telecommunications.

Author details

Maurizio Casalino

Address all correspondence to: maurizio.casalino@na.imm.cnr.it

Institute for Microelectronics and Microsystems (IMM) of the Italian National Research Council, Naples, Italy

References

[1] Jalali B, Fathpour S: Silicon photonics. J. Lightwave Technol. 2006;**24**:4600–4615.

[2] Paniccia M: Integrating silicon photonics. Nat. Photon. 2010;**4**:498–499.

[3] Kang Y, Mages P, Clawson AR, Yu PKL, Bitter M, Pan Z, Pauchard A, Hummel S, Lo YH: Fused InGaAs–Si Avalanche photodiodes with low noise performances. IEEE Photon. Tech. Lett. 2002;**14**:1593–1595.

[4] BelingA, Campbell J: InP-based high-speed photodetectors. J. Lightwave Technol. 2009; **27**:343–355.

[5] Koester SJ, Schaub JD, Dehlinger G, Chu, JO: Germanium-on-SOI infrared detectors for integrated photonic applications. IEEE J. Sel. Top. Quantum Electron. 2006;**12**: 1489–1502.

[6] Harame DL, Koester SJ, Freeman G, Cottrel P, Rim K, Dehlinger G, Ahlgren D, Dunn JS, Greenberg D, Joseph A, Anderson F, Rieh JS, Onge SAST, Coolbaugh D, Ramachandran V, Cressler JD, Subbanna S: The revolution in SiGe: impact on device electronics. Appl. Surf. Sci. 2004;**224**:9–17.

[7] Jones R, Park HD, Fang AW, Bowers JE, Cohen O, Raday O, Paniccia MJ: Hybrid silicon integration. J. Mater. Sci. Mater. Electron. 2009;**20**:3–9.

[8] Eng PC, Sung S, Ping B: State-of-the-art photodetectors for optoelectronic integration at telecommunication wavelength. Nanophotonics. 2015;**4**:277–302.

[9] Michel J, Liu J, Kimerling LC: High-performance Ge-on-Si photodetectors. Nat. Photon. 2010;4:527–534.

[10] Kang Y, Liu H-D, Morse M, Paniccia MJ, Zadka M, Litski S, Sarid G, Pauchard A, Kuo Y-H, Chen H-W, Zaoui WS, Bowers JE, Beling A, McIntosh DC, Zheng X, Campbell JC: Monolithic germanium/silicon avalanche photodiodes with 340GHz gain–bandwidth product. Nat. Photon. 2009;3:59–63.

[11] Vivien L, Osmond J, Fédéli J-M, Marris-Morini D, Crozat P, Damlencourt J-F, Cassan E, Lecunff Y, Laval S: 42 GHz p.i.n Germanium photodetector integrated in a silicon-on-insulator waveguide. Opt. Express. 2008;**17**:6252–6257.

[12] Wang J, Lee S: Ge-photodetectors for Si-based optoelectronic integration. Sensors. 2011;11:696–718.

[13] Alduino A, Liao L, Jones R, Morse M, Kim B, Lo W-Z, Basak J, Koch B, Liu H-F, Rong H, Sysak M, Krause C, Saba R, Lazar D, Horwitz L, Bar R, Litski S, Liu A, Sullivan K, Dosunmu O, Na N, Yin T, Haubensack F, Hsieh I-W, Heck J, Beatty R, Park H, Bovington J, Lee S, Nguyen H, Au H, Nguyen K, Merani P, Hakami M, Paniccia MJ: Demonstration of a high speed 4-channel integrated silicon photonics WDM link with hybrid silicon lasers. Hot Chips. 2010;22:Session 3.

[14] Narasimha A, Analui B, Balmater E, Clark A, Gal T, Guckenberger D, Gutierrez S, Harrison M, Ingram R, Koumans R, Kucharski D, Leap K, Liang Y, Mekis A, Mirsaidi S, Peterson M, Pham T, Pinguet T, Rines D, Sadagopan V, Sleboda TJ, Song D, Wang Y, Welch B, Witzens J, Abdalla S, Gloeckner S, De Dobbelaere P: A 40-Gb/s QSFP optoelectronic transceiver in a 0.13 μm CMOS silicon-on-insulator technology. In: Proceeding of the Optical Fiber Communications Conference (OFC); 2008; OMK7.

[15] Alloatti L, Srinivasan SA, Orcutt JS, Ram RJ: Waveguide-coupled detector in zero-change complementary metal-oxide-semiconductor. Appl. Phys. Lett. 2015;107:041104.

[16] Meng H, Atabaki A, Orcutt JS, Ram RJ: Sub-bandgap polysilicon photodetector in zero-change CMOS process for telecommunication wavelength. Opt. Express. 2015;23: 32643–32653.

[17] Casalino M, Coppola G, De La Rue RM, Logan DF: State-of-the-art all-silicon sub-bandgap photodetectors at telecom and datacom wavelengths. Laser Photon. Rev. 2016:10;895–921.

[18] Berini P, Olivieri S, Chen C: Thin Au surface plasmon waveguide Schottky detectors on p-Si. Nanotechnology. 2012;23:444011.

[19] Akbari A, Tait RN, Berini P: Surface plasmon waveguide Schottky detector. Opt. Express. 2010;18:8505–8514.

[20] Zhu S, Chu HS, Lo GQ, Bai P, Kwong DL: Waveguide-integrated near-infrared detector with self-assembled metal silicide nanoparticles embedded in a silicon p-n junction. Appl. Phys. Lett. 2012;100:061109.

[21] Sobhani A, Knight MW, Wang Y, Zheng B, King NS, Brown LV, Fang Z, Nordlander P, Halas NJ: Narrowband photodetection in the near-infrared with a plasmon-induced hot electron device. Nat. Commun. 2013;4:1643.

[22] Knight MW, Sobhani H, Nordlander P, Halas NJ: Photodetection with active optical antennas. Science. 2011;332:702–704.

[23] Amirmazlaghani M, Raissi F, Habibpour O, Vukusic J, Stake J: Graphene-Si Schottky IR detector. IEEE J. Quant. Electron. 2013;49:589–594.

[24] Kimata M, Ueno M, Yagi H, Shiraishi T, Kawai M, Endo K, Kosasayama Y, Sone T, Ozeki T, Tsubouchi N: PtSi Schottky-barrier infrared focal plane arrays. Opto-Electron. Rev. 1998;**6**:1–10.

[25] Casalino M, Sirleto L, Iodice M, Coppola G. Silicon photodetectors: the challenge of detecting near-infrared light. In: Gateva S editor. Photodetectors. InTech; 2012. p. 51–76. DOI: 10.5772/36014..

[26] Fowler RH: The analysis of photoelectric sensitivity curves for clean metals at various temperatures. Phys. Rev. 1931;38:45–56.

[27] Cohen J, Vilms J, Archer RJ: Investigation of Semi-conductor Schottky Barriers for Optical Detection and Cathodic Emission. Air Force Cambridge Research Labs. 1968; Report No. 68–0651.

[28] Elabd H, Kosonocky WF: Theory and measurements of photoresponse for thin film Pd2Si and PtSi infrared Schottky-barrier detectors with optical cavity. RCA Rev. 1982;**43**: 569–589.

[29] Stuart R, Wooten F, Spicer WE: Monte Carlo calculations pertaining to the transport of hot electrons in metals. Phys. Rev. 1964;**135**:A495–A505.

[30] Czernik A, Palm H, Cabanski W, Schulz M, Suckow U: Infrared photoemission of holes from ultrathin (3–20 nm) Pt/Ir-compound silicide films into silicon. Appl. Phys. 1992;**55**:180–191.

[31] Sellai A, Dawson P: Monte Carlo calculations of quantum yield in inhomogeneous PtSi/p-Si Schottky barriers. Semicond. Sci. Technol. 1998;**13**:700–704.

[32] Scales C, Berini P: Thin-film Schottky barrier photodetector models. IEEE J. Quant. Electron. 2010;**46**:633–643.

[33] Vickers VE: Model of Schottky barrier hot-electron-mode photodetection. Appl. Opt. 1971;**10**:2190–2192.

[34] Casalino M: Internal photoemission: theory revisited and theoretical limitations on the performance of near-infrared silicon Schottky photodetectors. IEEE J. Quant. Electron. 2016;**52**:4000110.

[35] Sze SM, Kwok KN. Physics of Semiconductor Devices. New York: Wiley; 2006.

[36] Donati S. Photodetectors: Devices, Circuits and Applications. New Jersey: Prentice Hall PTR; 1999.

[37] Esper J, Panetta P, Ryschkewitsch M, Wiscombe W, Neeck S: NASA-GSFC Nano-satellite technology for earth science missions. Acta Astronaut. 2000;**46**:287–296.

[38] Daffara C, Pampaloni E, Pezzati L, Barucci M, Fontana R: Scanning multispectral IR reflectography SMIRR: an advanced tool for art diagnostics. Acc. Chem. Res. 2010;**43**:847.

[39] Kimata M, Denda M, Yutani N, Iwade S, Tsubouchi N: A 512/spl times/512-element PtSi Schottky-barrier infrared image sensor. IEEE J. Solid-State Circ. 1987;**22**:1124–1129.

[40] Casalino M, Sirleto L, Moretti L, Della Corte F, Rendina I: Design of a silicon resonant cavity enhanced photodetector based on the internal photoemission effect at 1.55 μm. J. Opt. A Pure Appl. Opt. 2006;**8**:909–913.

[41] Casalino M, Sirleto L, Moretti L, Gioffrè M, Coppola G, Iodice M, Rendina I: Back-illuminated silicon resonant cavity enhanced photodetector at 1550 nm. Physica E. 2009;**41**:1097–1101.

[42] Casalino M, Sirleto L, Moretti L, Gioffrè M, Coppola G, Rendina I: Silicon resonant cavity enhanced photodetector based on the internal photoemission effect at 1.55 micron: fabrication and characterization. Appl. Phys. Lett. 2008;**92**:251104.

[43] Casalino M, Coppola G, Gioffrè M, Iodice M, Moretti L, Rendina I, Sirleto L: Silicon technology compatible photodetectors at 1.55 μm. J. Lightwave Technol. 2010;**28**:3266.

[44] Casalino M, Coppola G, Iodice M, Rendina I, Sirleto L: Critically coupled silicon Fabry-Perot photodetectors based on the internal photoemission effect at 1550 nm. Opt. Express. 2012;**20**:12599–12609.

[45] Desiatov B, Goykhman I, Mazurski N, Shappir J, Khurgin JB, Levy U: Plasmonic enhanced silicon pyramids for internal photoemission Schottky detectors in the near-infrared regime. Optica. 2015;**2**:335–338.

[46] Zhu S, Yu MB, Lo GQ, Kwong DL: Near-infrared waveguide-based nickel silicide Schottky-barrier photodetector for optical communications. Appl. Phys. Lett. 2008; 92:081103.

[47] Zhu S, Lo GQ, Kwong DL: Low-cost and high-speed SOI waveguide-based silicide schottky-barrier MSM photodetectors for broadband optical communications. IEEE Photon. Technol. Lett. 2008;**20**:1396–1398.

[48] Casalino M, Sirleto L, Iodice M, Saffioti N, Gioffrè M, Rendina I, Coppola G:Cu/p-Si Schottky barrier-based near-infrared photodetector integrated with a silicon-on-insulator waveguide. Appl. Phys. Lett. 2010;**96**:241112.

[49] Casalino M, Iodice M, Sirleto L, Rendina I, Coppola G: Low dark current silicon-on-insulator waveguide metal-semiconductor-metal photodetector based on internal photoemission effect at 1550 nm. J. Appl. Phys. 2013;**114**:153103.

[50] Casalino M, Iodice M, Sirleto L, Rendina I, Coppola G: Asymmetric MSM sub-bandgap all-silicon photodetector with low dark current. Opt. Express. 2013;**21**: 28072–28082.

[51] Zali AR, Moravvej-Farshi MK: Nonidealities and dark current in IR photodetector based on silicide-nanolayer Schottky barrier integrated into a Si microring resonator. IEEE J. Quant. Electron. 2015;**51**:4000108.

[52] Hosseinifar M, Ahmadi V, Ebnali-Heidari M: Si-Schottky photodetector based on metal stripe in slot-waveguide microring resonator. IEEE Photon. Technol. Lett. 2016;28: 1363–1366.

[53] Huang YP, Wang LA: In-line silicon Schottky photodetectors on silicon cored fibers working in 1550 nm wavelength regimes. Appl. Phys. Lett. 2015;**106**:191106.

[54] Maier SA: Plasmonics: Fundamentals and Applications. New York: Springer; 2007.

[55] Akbari A, Berini P: Schottky contact surface-plasmon detector integrated with an asymmetric metal stripe waveguide. Appl. Phys. Lett. 2009;**95**:021104.

[56] Olivieri A, Akbari A, Berini P: Surface plasmon waveguide Schottky detectors operating near breakdown. Phys. Status Solidi RRL. 2010;**4**:283–285.

[57] Scales C, Breukelaar I, Charbonneu R, Berini P: Infrared performance of symmetric surface-plasmon waveguide Schottky detectors in Si. J. Lightwave Technol. 2011;29: 1852–1860.

[58] Zhu S, Lo GQ, Kwong DL: Theoretical investigation of silicide Schottky barrier detector integrated in horizontal metal-insulator-silicon-insulator-metal nanoplasmonic slot waveguide. Opt. Express. 2011;**19**:15843–15854.

[59] Knight MK, Wang Y, Urban AS, Sobhani A, Zheng BY, Nordlander P, Halas NJ: Embedding plasmonic nanostructure diodes enhances hot electron emission. Nanoletters. 2013;13:1687–1692.

[60] Goykhman I, Desiatov B, Khurgin J, Shappir J, Levy U: Waveguide based compact silicon Schottky photodetector with enhanced responsivity in the telecom spectral band. Opt. Express. 2012;**20**: 28594–28602.

[61] Goykman I, Desiatov B, Khurgin J, Shappir J, Levy U: Locally oxidized silicon surface-plasmon Schottky detector for telecom regime. Nano Lett. 2011;11:2219–2224.

[62] Fathauer RW, Iannelli JM, Nieh CW, Hashimoto S: Infrared response from metallic particles embedded in a single-crystal Si matrix: the layered internal photoemission sensor. Appl. Phys. Lett. 1990;**57**:1419–1421.

[63] Fathauer RW, Dejewski SM, George T, Jones EW, Krabach TN, Ksendzov A: Infrared photodetectors with tailorable response due to resonant plasmon absorption in epitaxial silicide particles embedded in silicon. Appl. Phys. Lett. 1993;**62**:1774–1776.

[64] Stuart RH, Hall DG: Island size effects in nanoparticle-enhanced photodetectors. Appl. Phys. Lett. 1998;**73**:3815–3817.

[65] Schaadt DM, Feng B, Yu ET: Enhanced semiconductor optical absorption via surface plasmon excitation in metal nanoparticles. Appl. Phys. Lett. 2005;**86**:063106.

[66] Raissi F: A possible explanation for high quantum efficiency of PtSi/porous Si Schottky detectors. IEEE Trans. Electron. Dev. 2003;**50**:1134.

[67] Fukuda M, Aihara T, Yamaguchi K, Ling YY, Miyaji K, Tohyama M: Light detection enhanced by surface plasmon resonance in metal film. Appl. Phys. Lett. 2010;**96**: 153107.

[68] Nazirzadeh MA, Atar FB, Turgut BB, Okyay AK: Random sized plasmonic nanoantennas on silicon for low-cost broad-band near-infrared photodetection. Sci. Rep. 2014;**4**:7103.

[69] Muehlbrandt S, Melikyan A, Harter T, Kohnle K, Muslija A, Vincze P, Wolf S, Jokobs P, Fedoryshyn Y, Freude W, Leuthold J, Koos C, Kohl M: Silicon-plasmonic internal-photoemission detector for 40 Gbit/s data reception. Optica. 2016;**3**:741–747.

[70] Novoselov KS, Fal'ko VI, ColomboL, Gellert PR, Schwab MG, Kim K: A roadmap for graphene. Nature. 2012;**490**:192–200.

[71] Dawlaty J, Shivaraman S, Strait J, George P, Chandrashekhar M, Rana F, Spencer MG, Veksler D, Chen Y: Measurement of the optical absorption spectra of epitaxial graphene from terahertz to visible. Appl. Phys. Lett. 2008;**93**:131905-1-13.

[72] Sensale-Rodriguez B, Yan R, Kelly MM, Fang T, Tahy K, Hwang WS, Jena D, Liu L, Xing HG: Efficient terahertz electro-absorption modulation employing graphene plasmonic structures. Appl. Phys. Lett. 2012;**101**:261115.

[73] Chen C-C, Aykol M, Chang C-C, Levi AFJ, Cronin SB: Graphene-silicon Schottky diodes. Nano Lett. 2011;**11**:1863–1867.

[74] Goykhman I, Sassi U, Desiatov B, Mazurski N, Milana S, de Fazio D, Eiden A, Khurgin J, Shappir J, Levy U, Ferrari AC: On-chip integrated, silicon–graphene plasmonic Schottky photodetector with high responsivity and avalanche photogain. Nano Lett. 2016;16:3005–3013.

[75] Levy U, Grajower M, Goncalves PAD, Mortensen NA, Khurgin JB: Plasmonic silicon Schottky photodetectors: the physics behind graphene enhanced internal photoemission. APL Photon. 2017;**2**:026103.

[76] Padovani FA, Stratton R: Field and thermionic-field emission in Schottky barriers. Solid State Electron. 1966;**9**:695–707.

[77] Vabbina P, Choudhary N, Chowdhury A-A, Sinha R, Karabiyik M, Das S, Choi W, Palaoi N, Pala N: Highly sensitive wide bandwidth photodetector based on internal photo-emission in CVD grown p-type MoS2/graphene Schottky junction. ACS Appl. Mater. Interfaces. 2015;**7**:15206–15213.